Microchimica Acta (2023) 190:328
https://doi.org/10.1007/s00604-023-05906-9

ORIGINAL PAPER

MXene-sensitized electrochemiluminescence sensor for thrombin activity detection and inhibitor screening

Zijie Deng[1,2] · Xueping Tan[1,2] · Dongnan Guo[1,2] · Jing Zhang[1,2] · Dan Xu[1,2] · Xiaofang Hou[1,2] · Sicen Wang[1,2] · Junbo Zhang[3] · Fen Wei[1,2] · Dongdong Zhang[1,2]

Received: 11 April 2023 / Accepted: 7 July 2023 / Published online: 27 July 2023

Abstract

Thrombin, a crucial enzyme involved in blood coagulation and associated diseases, requires accurate detection of its activity and screening of inhibitors for clinical diagnosis and drug discovery. To address this, an electrochemiluminescence (ECL) method was developed to detect thrombin activity based on the sensitization of $Ti_3C_2T_x$ MXene, which could sensitize the $Ru(bpy)_3^{2+}$ ECL system greatly. The thrombin-cleavable substrate bio-S-G-R-P–V-L-G-C was used as recognizer to evaluate the activity of thrombin. Under the optimal conditions, the limit of detection for thrombin in serum was 83 pU/mL (S/N = 3) with a linear range from 0.1 nU/mL to 1 μU/mL. Moreover, the developed ECL biosensor was employed to screen for thrombin inhibitors from Artemisiae argyi Folium. Four potential thrombin inhibitors (isoquercitrin, nepetin, L-camphor, L-borneol) were screened out with inhibition rates beyond 50%, among which isoquercitrin had the best inhibition rate of 90.26%. Isoquercitrin and nepetin were found to be competitive inhibitors of thrombin, with K_i^{app} values of 0.91 μM and 2.18 μM, respectively. Molecular docking results showed that these compounds could interact with the active sites of thrombin through hydrogen bonds including ASP189, SER195, GLY216, and GLY219. The electrochemical biosensor constructed provides a new idea for the detection of thrombin activity and screening of its inhibitors.

Keywords Electrochemiluminescence · Thrombin activity · MXene · Thrombin inhibitors · Artemisiae argyi Folium

Introduction

Thrombin is a multi-functional serine proteolytic enzyme and is the key to blood clotting [1–3]. The representation of thrombin activity may provide a more precise assessment of its biological function and disease status than the measurement of thrombin concentration [4, 5]. Therefore, monitoring thrombin's activity is beneficial for early diagnosis and treatment of diseases and individualized medication guidance.

Through literature review, there are various methods for the detection of thrombin activity: direct detection and indirect detection [6]. Direct detection means that thrombin directly acts on the substrate peptide segment to produce signal changes, including fluorescent [7] and ultraviolet method [8]. The advantages are high accuracy and sensitivity [9], but the disadvantages are high cost. Indirect detection has advantages of simplicity and low cost, but its disadvantages are low accuracy and sensitivity [10, 11]. Electrochemiluminescence (ECL) integrates the advantages of chemiluminescence and electrochemistry: high sensitivity, good reproducibility, and simple use, among others, providing a new idea for the determination of thrombin activity [12].

Tris(bipyridine)ruthenium(II)/tri-n-propylamine($Ru(bpy)_3^{2+}$/TPA) system has been widely used for ECL detection due to its good stability and strong signal [13]. However, the strong water solubility of $Ru(bpy)_3^{2+}$ limits its utilization in ECL applications.

Zijie Deng and Xueping Tan contributed equally.

✉ Xiaofang Hou
houxiaofang@mail.xjtu.edu.cn

✉ Sicen Wang
wangsc@mail.xjtu.edu.cn

✉ Junbo Zhang
zhangjunbo@xjtufh.edu.cn

1 School of Pharmacy, Health Science Center, Xi'an Jiaotong University, 76 Yanta West Road, Xi'an 710061, China

2 Shaanxi Engineering Research Center of Cardiovascular Drugs Screening and Analysis, Xi'an 710061, China

3 Department of Peripheral Vascular Disease, The First Affiliated Hospital of the Medical College of Xi'an Jiaotong University, 277 Yanta West Road, Xi'an 710061, China

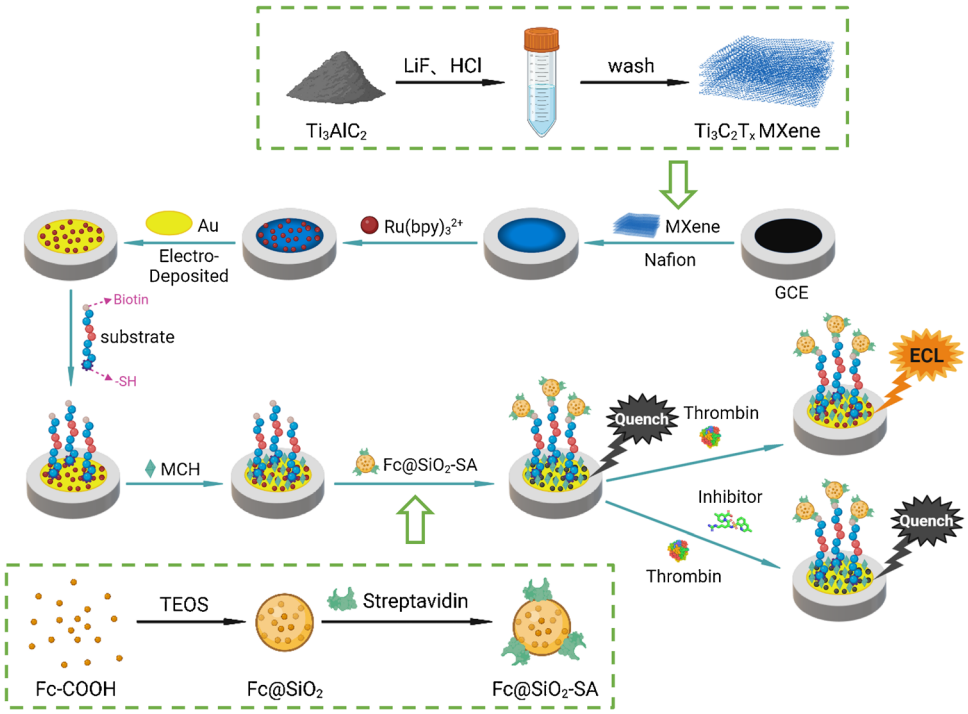

Scheme 1 Scheme for the construction of a biosensor for thrombin activity detection and inhibitor screening

Thus, solving its immobilization problem is necessitated [14]. As a new class of two-dimensional carbide or nitride, MXene has excellent conductance, stability, and hydroxyl and oxygen groups on its surface that can promote surface modification and realize stable intercalation of functional molecules [15]. Therefore, ultrathin two-dimensional MXene nanosheets were selected to solve the immobilization problem of $Ru(bpy)_3^{2+}$.

In this work, a highly sensitive ECL method for the determination of thrombin activity was developed using the sensitization effect of MXene (Scheme 1). The first step is to prepare MXene and ferrocene@SiO_2-streptavidin (Fc@SiO_2-SA) nanoparticles (see the "Experimental methods" section for details). Then, MXene was modified on the surface of glassy carbon electrode (GCE) using Nafion. Gold nanoparticles were then modified on the electrode. The substrate peptide was attached to the GCE by Au–S bond, and the non-specific adsorption site was blocked with mercaptohexanol (MCH). Through the interaction between SA and biotin, Fc@SiO_2-SA nanoparticles prepared were connected to the surface of GCE to form a biosensor. The presence of active thrombin specifically cleaved substrate peptides, resulting in the shedding of Fc@SiO_2-SA nanoparticles and a significant increase in ECL intensity. Furthermore, in the presence of the inhibitor, thrombin was unable to lyse the peptide, leading to no significant change in ECL strength. The biosensor was utilized to measure human thrombin activity and screen for potential thrombin inhibitors.

Artemisiae argyi Folium (AAF) is a kind of traditional Chinese herbal medicine, which has been proved to contain rich natural active substances. Volatile oil is the main active substance in AAF, which has been shown to have antioxidant, antibacterial, and anti-inflammatory effects [16]. Studies have also found that AAF can improve intestinal immunity and antioxidant capacity [17, 18]. In this study, 10 active components of AAF (cebutathrin, cineolin, isoquercitrin, nepetin, eupatilin, β-sitosterol, 4-terpenenol, α-terpineol, L-camphor, L-borneol) were selected to screen potential thrombin inhibitors using the developed ECL biosensors.

Experiment

Materials and reagents

Titanium Aluminum Carbide (Ti_3AlC_2, 99.9%), Nafion 117(5%), hydrogen tetrachloroaurate(III) trihy-drate ($HAuCl_4 \cdot 3H_2O$, 99.9%), terpyridine ruthenium chloride hexahydrate ($Ru(bpy)_3Cl_2 \cdot 6H_2O$, 98%), hemoglobin (Hb), lysozyme, and human albumin (HSA, 96–99%) were purchased from Shanghai Macklin Biochemical Co., Ltd. (Shanghai, China). Tris (4,4'-dicarboxylicacid-2,2'-bipyridyl) rutheniuM(II) dichloride ($Ru(dcbpy)_3Cl_2$, 98%) was purchased from Suzhou Suna Tech Inc. (Suzhou, China). Streptavidin (SA) and human immunoglobulin (IgG, 50%) were obtained from Beijing Solarbio Science and Technology Co., Ltd. (Beijing, China). The thrombin polypeptide substrate was synthesized and purified by Sangon Biotech Co., Ltd. (Shanghai, China) with the sequence of bio-S-G-R-P–V-L-G-C. The fluorescent substrate of chymotrypsin

BOC-Val-Pro-Arg-AMC (98%, BOC: t-Butyloxycarbonyl; AMC: 7-Amino-4-methylcoumarin.) was purchased from AAT Bioquest (USA). Jaceosidin (Jac), cineole (Cin), isoquercitrin (Iso), nepetin (Nep), eupatilin (Eup), and β-sitosterol (β-Sit) were provided by Chengdu Yirui Biotechnology Co., Ltd. (Chengdu, China). 4-terpenenol (Ter) and α-terpineol (α-Ter) were provided by Shanghai Bepharm Science&Technology Co., Ltd. (Shanghai, China). L-camphor (L-Cam) and L-borneol (L-Bor) were provided by Shanghai Yuan-fan Biotechnology Co., Ltd. (Shanghai, China). All chemical reagents were analytical grade, and ultrapure water with a resistivity of 18.2 MΩ cm was used throughout the experiment.

Instrument

A glassy carbon electrode (GCE, Φ = 3 mm) was used as the working electrode, an Ag/AgCl (saturated KCl) electrode as the reference electrode, and a platinum wire (Pt) as the counter electrode in a standard three-electrode system. The ECL measurement was performed on the MPI-A/B ECL analyzer (China Xi'an Remax Electronic Science and Technology Co., Ltd., Xi'an, China) in a dark room at 25 ℃. Cyclic voltammetry (CV) and electrochemical impedance spectroscopy (EIS) measurements were performed on CH1660E electrochemistry workstation (Shanghai CH Instrument, China). Transmission electron microscope (TEM, FEI-F20, Thermo Fisher Scientific, American) and scanning electron microscope (SEM, ZEISS sigma 300, Carl Zeiss AG, Germany) were used to record the morphology of different composite materials. X-ray photoelectron spectroscopy (XPS) was performed on a Thermo Scientific Escalab 250Xi Instrument (Thermoelectricity Instruments, USA). Fourier transform infrared spectrometry (FT-IR) was conducted on a Thermo IRTracer 100 FTIR spectrometer using KBr pellets (American). The zeta potential and particle size distribution were conducted by a Zetasizer Nano ASE analyzer (Malvern, UK). An ultraviolet spectrophotometer (UV 1600, Fuli Instrument, Zhejiang) and fluorescence spectrophotometer (RF-6000, Shimadzu, Japan) was used to obtain the ultraviolet–visible (UV–Vis) spectrum and fluorescence spectrum. Fluorescence and ECL results were compared using a multi-function microplate reader system (SuPerMax-3000M2, Flash, Shanghai) in the recovery experiment.

Preparation of $Ti_3C_2T_x$ MXene and sensitization test

$Ti_3C_2T_x$ MXene was synthesized by etching Ti_3AlC_2 with HF. First, 2.0 g LiF was dissolved in 20 mL 12 M hydrochloric acid and stirred evenly. Ti_3AlC_2 (1 g) was added incrementally and stirred at 45 ℃ for 24 h. The etching solution was discarded by centrifugation, and the precipitate was washed twice with 1 mM HCl and then with ultrapure water (pH 6). The precipitation was collected by centrifugation and vacuum freeze-drying to obtain $Ti_3C_2T_x$ MXene powder. (3-Aminopropyl)triethoxysilane (APTES) was stirred with $Ti_3C_2T_x$ MXene for 12 h to get NH_2-MXene.

$Ti_3C_2T_x$ MXene (10 mg/mL) was dispersed in Nafion solution (1% w/v) (1:1, v/v), to form Nafion/MXene mixture, and then, ultrasonic dispersion for 20 min resulted in the uniform Nafion/MXene dispersion. Then, 5 μL prepared Nafion/MXene and Nafion solution (0.5% w/v) were separately added to the surface of GCE. After drying, 20 μL 10 mM $Ru(bpy)_3^{2+}$ solution was added to the surface of GCE, and the excess $Ru(bpy)_3^{2+}$ was removed to obtain the modified electrode.

Preparation of Fc@SiO_2 nanocomposites

Fc@SiO_2 nanocomposites were successfully synthesized by reversed-phase microemulsion method. Firstly, 7.5 mL cyclohexane, 1.8 mL n-hexanol, and 1.77 mL trilatone X-100 were mixed and stirred for 30 min. A 400 μL 0.2 M Fc-COOH was added to the above solution and stirred for 30 min to form a stable W/O system. Then, 100 μL tetraethyl orthosilicate (TEOS) and 60 μL $NH_3{\cdot}H_2O$ (30% w/v) were slowly added and stirred continuously for 24 h. After the reaction was completed, Fc@SiO_2 nanoparticles were separated from the W/O system by adding 10 mL acetone and centrifugation at 6000 r/min for 30 min. Finally, the precipitation was washed with water and ethanol several times, and Fc@SiO_2 was stored in 1 mL anhydrous ethanol.

Preparation of Fc@SiO_2@SA

Fc@SiO_2 nanoparticles were connected with streptavidin (SA) according to Dong et al. [19]. Firstly, the prepared 1 mL Fc@SiO_2 suspension was diluted to 5 mL with anhydrous ethanol, and 400 μL APTES was added stirred for 4 h. The product was collected by centrifugation (12,000 rpm, 10 min) and washed several times with water and ethanol. Then, 5 mL of 5% (w/v) glutaraldehyde solution was added and stirred for 4 h. The product was washed again with water and dispersed in 2 mL of ultrapure water. Finally, 200 μL SA solution (1.0 mg /mL, 0.01 M PBS) was added, stirred for 4 h, and centrifuged with PBS (0.01 M pH 7.4) for several times to obtain Fc@SiO_2@SA, which was dispersed in 1 mL PBS (0.01 M pH 7.4) and stored at 4 ℃ for use.

Construction of the ECL sensor

The electrode underwent polishing using 0.05 μm Al_2O_3 polishing powder on a chamois cloth until it achieved a mirror-like surface. Afterwards, it was rinsed with ultrapure water and dried using nitrogen gas. A solution containing 30 mg/mL of MXene dispersion was combined with 0.75% Nafion

(w/v) at a 1:1 volume ratio. After 30 min of sonication, the resulting mixture was evenly spread over the surface of a GCE and allowed to dry at room temperature. Then, 20 μL of 10 mM $Ru(bpy)_3Cl_2$ solution was added and dried at 60 ℃. Excess $Ru(bpy)_3Cl_2$ was washed away and dried. Next, the nano-gold film was modified by electrodeposition, and then, 10 μL 0.5 mg/mL thrombin substrate was added to the surface of the electrode by drops and incubated at 4 ℃ for 18 h away from light. After that, the excess substrate was removed, and 10 μL 1 mM MCH was dripped onto the electrode surface and incubated for 1 h at 4 ℃ in the dark to block the excess non-specific adsorption sites. Then, 10 μL $Fc@SiO_2@SA$ solution was added to the electrode and incubated at 4 ℃ for 18 h in the dark. Finally, the $Ru@MXene/Fc@SiO_2@SA$ ECL biosensor was obtained.

Determination of thrombin activity in human serum

Blood sample (5 mL) from a healthy volunteer was centrifuged at 12,000 rpm for 15 min, and the supernatant was collected and diluted 100 times as the prepared serum. Thrombin solution in PBS buffer (pH 7.4 0.1 M) (1 mL) with different activity units (1.00×10^{-9} U/mL, 1.00×10^{-8} U/mL, 1.00×10^{-7} U/mL) was spiked into the prepared serum (1 mL) separately. The mixture (10 μL) was added onto the as-prepared ECL biosensor at 37 ℃ for 1 h followed by washing completely with PBS. The ECL response was recorded from − 0.1 to 0.6 V at a scan rate of 100 mV/s. The voltage of the photomultiplier tube (PMT) was set at − 600 V. CV and EIS were collected in a solution that contained 0.1 M KCl and 5 mM $[Fe(CN)_6]^{3-}/[Fe(CN)_6]^{4-}$(1:1). The CV measurement range was − 0.1 to 0.6 V, and the scan rate was 100 mV/s. The EIS measurement was performed from 0.1 Hz to 100 kHz, 25.0 mV amplitude, and 0.23 V electrode potential.

Screening of thrombin inhibitors in Artemisiae argyi Folium

Argatroban (10 nM, 40 μL) and 10 tested compounds (Jac, Cin, Iso, Nep, Eup, β-Sit, Ter, α-Ter, L-Cam, and L-Bor) (1 μM, 40 μL) were separately incubated with 1 μU/mL thrombin at 37 ℃ for 10 min. Then, each mixture was dropped on the surface of the electrode to carry out the enzymatic reaction. After incubation at 37 ℃ for 60 min, the reaction on the electrode surface was terminated, and the ECL signal was recorded. Meanwhile, in order to verify the results, the commercial fluorescence method was also performed. Different compounds were separately mixed with thrombin solution and incubated at 37 ℃ for 10 min. Then, 50 μL 0.05 mg/mL substrate (Boc-Val-Pro-Arg-AMC) solution was added. After incubation at 37 ℃ for 60 min, the fluorescence intensities of the final solutions were recorded using a microplate reader at 380 nm excitation and 460 nm emission.

Determination of K_i value of potential inhibitors

First, different concentrations of substrates (1 ~ 64 μM, two-fold relationship between concentrations) were added on the biosensor and to calculate the K_m value of thrombin under the optimal conditions. Next, Arg (10 nM), Iso (1 μM), and Nep (1 μM) were mixed with 1 μU/mL thrombin and incubated at 37 ℃ for 10 min, respectively. Then, the above substrates (1 ~ 64 μM) were added on the biosensor and to calculate the K_i value of Arg (10 nM), Iso (1 μM), and Nep (1 μM), respectively.

Molecular docking assay

The molecular docking assay was carried out using AutoDock 4.2 (Scripps Research Institute, USA), where the crystal structure of thrombin (PDB ID = 3 RM2) with a resolution of 1.23 Å was obtained from PDB.org. The ligand Hirudin variant-2 and water molecules were removed, and polar hydrogen atoms were added. The SDF formats of argatroban, isoquercitrin, nepetin, L-camphor, and L-borneol were converted into PDB format and output with OpenBabel 2.4 to ensure that the energy of the compound was minimized. After that, molecular docking was performed with AutoDock 4.2.

Results and discussion

Characterization of $Ti_3C_2T_x$ MXene

The structure and morphology of $Ti_3C_2T_x$ MXene were characterized by scanning electron microscopy (SEM). As shown in Fig. 1a, the SEM image of $Ti_3C_2T_x$ MXene shows an accordion-like layered structure [20, 21]. The results indicate that the material exhibits a favorable stripping effect. Figure 1b displays the X-ray diffraction (XRD) patterns of Ti_3AlC_2 and $Ti_3C_2T_x$ MXene. The results show that the peak (104) of Ti_3AlC_2 disappears in the X-ray diffraction pattern of $Ti_3C_2T_x$ MXene, indicating that the Al layer has been successfully removed after etching. Compared with Ti_3AlC_2, the (002) peak of $Ti_3C_2T_x$ MXene is shifted to a smaller angle due to the enlarged interlayer, which indicates that Ti_3AlC_2 has been successfully transformed into $Ti_3C_2T_x$ MXene [22, 23]. The Fourier transform infrared spectra (FT-IR) of Ti_3AlC_2 and $Ti_3C_2T_x$ MXene are shown in Fig. 1c. To be specific, -OH as surface-bonded functional groups, interlayer intercalated water molecules, or externally adsorbed water molecules trigger the absorption peaks at 3430 and 1633 cm^{-1}. The results indicate that Al has been

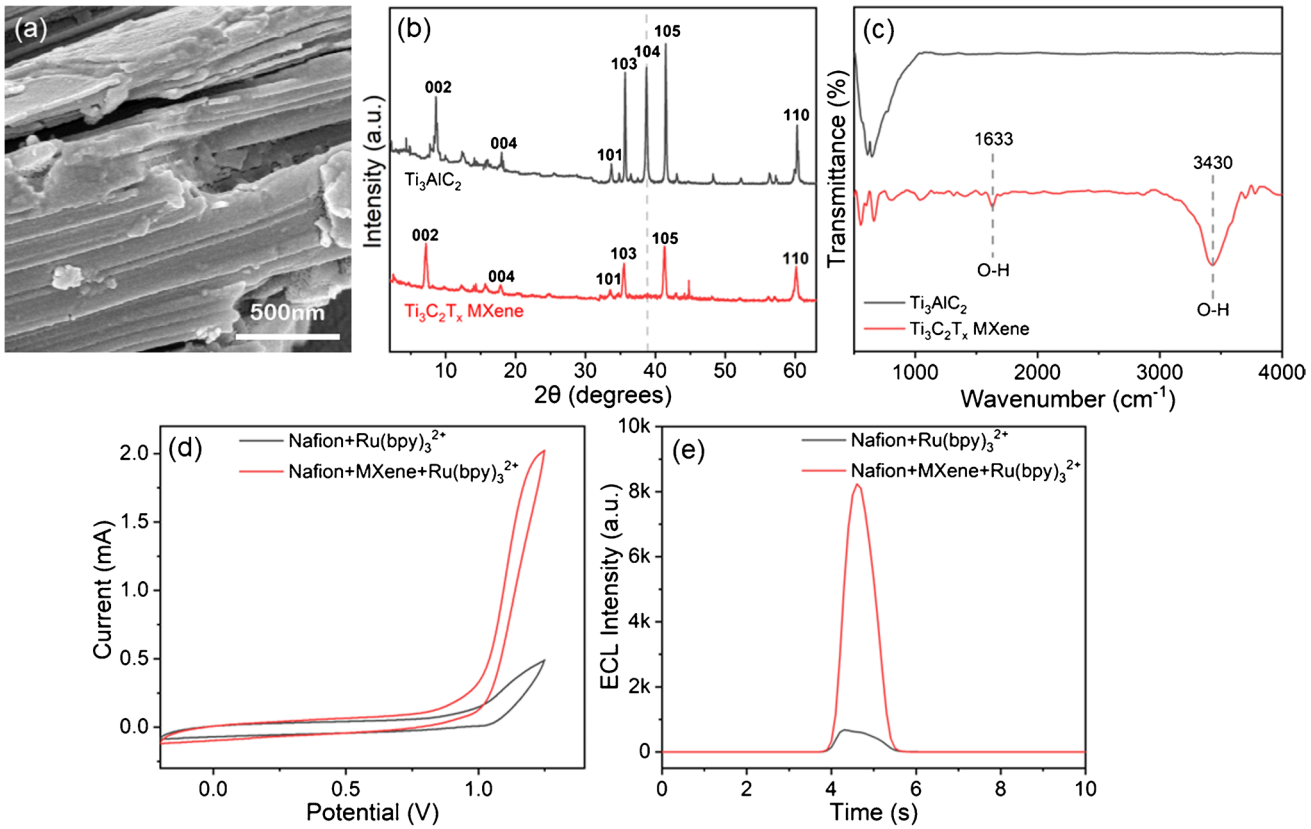

Fig. 1 Structure characterization of $Ti_3C_2T_x$ MXene synthesis process. **a** SEM of $Ti_3C_2T_x$ MXene; **b**, **c** XRD and FT-IR of Ti_3AlC_2, $Ti_3C_2T_x$ MXene; **d**, **e** CV and ECL curve of Nafion/$Ru(bpy)_3^{2+}$ and Nafion/MXene/$Ru(bpy)_3^{2+}$

successfully exfoliated and removed, exposing the interlayer -OH of $Ti_3C_2T_x$ MXene [24, 25]. The FT-IR analysis provides additional evidence of the successful synthesis of $Ti_3C_2T_x$ MXene.

The composition of $Ti_3C_2T_x$ MXene stripped powder was analyzed by X-ray photoelectron spectroscopy (XPS). The full spectrum of titanium (Ti), carbon (C), oxygen (O), and fluorine (F) is shown in Fig. S1(a). From Fig. S1(b), we can see that the Ti2p spectrum has six peaks at 454.42, 455.60, 458.53, 460.78, 463.85, and 464.81 eV, which belong to Ti-C 2p3; Ti 2p3; Ti–O, F 2p3; Ti 2p1; Ti-C 2p1; and Ti–O 2p1 bands, respectively. C1s spectrum (Fig. S1c) has three peaks at 281.14, 284.46, and 285.63 eV, belonging to C-Ti-T_x, C–C, and C-O bands, respectively. As shown in Fig. S1(d), there are five peaks in the O1s spectrum at 529.18, 529.99, 531.14, 532.34, and 533.68 eV, belonging to the O-Ti, C-Ti-O_x, C-Ti-$(OH)_x$, O–Al, and H_2O bands. These XPS results are consistent with Han et al. [26], Yang et al. [27], and Halim et al. [28], which indicate the successful preparation of MXene.

The results of sensitization effect of MXene are shown in Fig. 1d and e. The current (Fig. 1d) and the ECL intensity (Fig. 1e) of the Nafion/MXene modified electrode (red line) are enhanced about 4 and 12 times compared with the pure Nafion modified electrode (black line), which proves that MXene has good electrical conductivity and MXene has excellent fixation effect on $Ru(bpy)_3^{2+}$ [29, 30].

Characterization of Fc@SiO_2@SA

The characterization of Fc@SiO_2@SA information is displayed in Fig. S2. Figure S2(a) shows the TEM image of Fc@SiO_2@SA. It can be seen that Fc@SiO_2 is a spherical particle with a particle size of about 120 nm, which is uniform and smooth. SA with a particle size of about 40 nm is attached to the Fc@SiO_2 surface and provided good dispersion in water. Figure S2(b) shows the zeta potential changes during the synthesis of Fc@SiO_2@SA. The zeta potential changes from − 9.74 mV (Fc@SiO_2) to 1.29 mV (Fc@SiO_2-NH_2), which indicates the successful grafting of -NH_2 by APTES. After the connection of SA, the zeta potential value changes to − 4.81 mV. The results indicate the successful preparation of Fc@SiO_2@SA.

The UV–visible absorption spectra of SA, Fc, Fc@SiO_2, and Fc@SiO_2@SA are shown in Fig. S2(c). SA has an absorption peak at 290 nm. Fc@SiO_2 and Fc@SiO_2@SA

have two absorption peaks at 303 nm and 439 nm which are attributed to Fc. The peak at 303 nm represents π-π* transition and the peak at 439 nm due to the center transfer characteristics of Fc ligands. After the formation of Fc@SiO_2, the absorptions at 303 nm and 439 nm are further enhanced, which may be due to the core–shell structure of SiO_2 that exhibits Fc accumulation effect [31, 32].

The FT-IR spectra of SA, Fc, Fc@SiO_2, and Fc@SiO_2@SA are shown in Fig. S2(d), showing the functional groups in the synthesis process. The wide absorption band at 1219 ~ 1068 cm^{-1} is the antisymmetric stretching vibration peak of Si–O-Si, and the symmetric stretching vibration peak at 794 cm^{-1} and 449 cm^{-1} is the symmetric stretching vibration peak of Si–O, which proves that Fc@SiO_2 has good stability. Meanwhile, the double peaks of SA at 2920 cm^{-1} and 2665 cm^{-1} indicate that SA has been successfully combined to Fc. The above conclusions prove that the preparation of Fc@SiO_2@SA is successful.

Characterization of the ECL biosensor

The changes of current and voltage during the sensor preparation are characterized by cyclic voltammetry analysis (CV), as shown in Fig. 2a. First, a pair of REDOX peaks appeared at 0.29 V and 0.21 V at the unmodified GCE electrode, corresponding to the current of 4.06×10^{-5} A and -4.16×10^{-5} A, respectively. After modification of MXene@Nafion, due to the poor conductivity of Nafion [33, 34], the REDOX peak changes to 0.34 V and 0.18 V, the voltage difference increases significantly, and the current decreases significantly. After modification of $Ru(bpy)_3^{2+}$, the REDOX peak changes to 0.46 V and 0.14 V, and the current further decreases, possibly because $Ru(bpy)_3^{2+}$ obstructs the electron transport on the GCE surface. After electrodeposition of Au, the REDOX peaks are 0.30 V and 0.19 V, and the current is also significantly increased due to the strong conductivity of Au. After modification of the substrate and Fc@SiO_2@SA, the current decreases gradually because of the poor conductivity of the polypeptide and SiO_2. Once thrombin was present and specifically cut off the peptide, the current value increased due to Fc@SiO_2@SA nanocomposite away from the electrode. These results indicate that the construction of the ECL biosensor was successful.

Electrochemical impedance spectrum (EIS) is used to characterize the resistance changes during the sensor preparation, as shown in Fig. 2b. The main parameters include electrolyte solution (Rs), electrode surface transfer resistance (Ret), Warburg impedance (W), and double layer capacitance (CPE), where Ret reflects the change of electrode surface resistance. First, the unmodified GCE electrode had an extremely low Ret value of 53 Ω. After modification of MXene@Nafion and $Ru(bpy)_3^{2+}$, the Ret value increased to 2350 Ω and 4047 Ω due to the poor conductivity. When Au was electrodeposited, the strong conductivity of Au reduced the Ret value to 1418 Ω. Next, after the substrate and Fc@SiO_2@SA were attached, the Ret value increased to 4615 Ω and 5114 Ω due to the poor conductivity of them. Finally, when thrombin cut off the peptide, part of the Fc@SiO_2@SA left, and the Ret value decreased slightly to 4590 Ω. Therefore, the EIS results are consistent with CV, which further indicate the successful construction of the ECL biosensor.

Figure 2c shows the specific ECL behavior of the biosensor. The bare GCE and the one modified with MXene@Nafion do not show a significant ECL signal. After modification of $Ru(bpy)_3^{2+}$, an obvious ECL signal peak of 7486 a.u. appears. After Au electrodeposition, the ECL value decreased to 7031 a.u. When the substrate was incubated, the ECL value decreased further to 5717 a.u. due to the blocking effect of peptide. Next Fc@SiO_2@SA was connected, and the ECL value dropped to 117 a.u. due to the strong quenching effect of Fc@SiO_2@SA. Finally, when thrombin was added, the ECL signal increased to 4896 a.u. because part of Fc@SiO_2@SA was displaced. These results demonstrate the successful construction of the ECL biosensor.

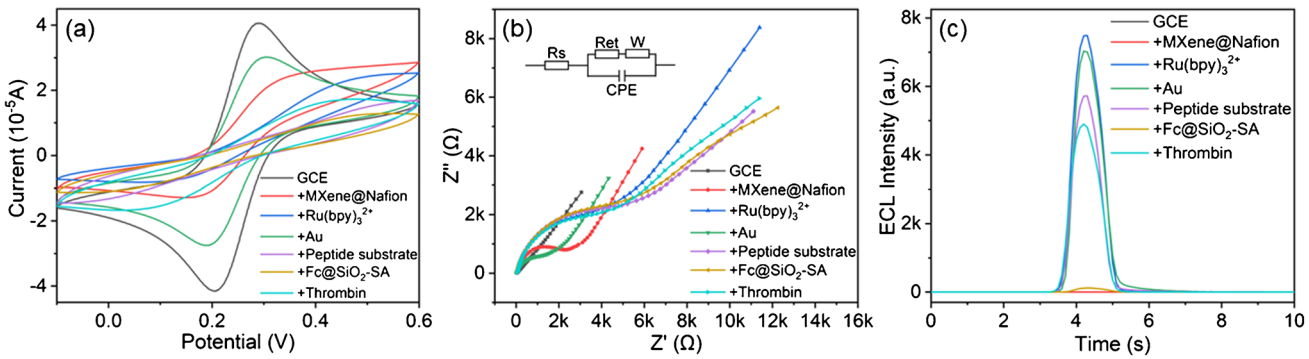

Fig. 2 Characterization diagram of ECL biosensor preparation process. **a** Cyclic voltammetry (CV); **b** electrochemical impedance spectroscopy (EIS); **c** electrochemical luminescence diagram (ECL)

Analytical performance of thrombin ECL biosensor

The "Optimization of the experimental conditions" section is shown in the Supplementary Material. The thrombin with different activities (1×10^{-10} U/mL ~ 1×10^{-6} U/mL) was detected under the optimal conditions to investigate the analytical performance of the sensor. Figure 3a–c show the ECL curves (a) and the linear curve (b) of different thrombin activities and selectivity (c) of the ECL sensor. The ECL value gradually increased with increasing thrombin activity. The ECL biosensor demonstrated a high level of accuracy with a linear regression equation of $y = 337.18x + 3420.43$ and a correlation coefficient (r) of 0.9998. In addition, the sensor displayed a low detection limit (LOD) of 8.3×10^{-11} U/mL (S/N = 3) for thrombin activity. The criterion for determination of the LOD is based on the 3σ/m criterion (where σ is the standard deviation of the blank or standard deviation of the intercept and m is the slope of the calibration plot). Figure 3c illustrates that the ECL biosensor displays a notably high response to thrombin, while ΔECL for HSA, IgG, Hb, and lysozyme is comparable to that of the blank control, indicating that the constructed ECL biosensor is specific to thrombin. The sensor also demonstrated a strong level of repeatability (Fig. 3d), with relative standard deviation (RSD) of 4.00% and 4.16% for five modified GCE electrodes before (red) and after (blue) incubation with thrombin. The precision of the ECL sensor was also investigated. As shown in Fig. 3e, the electrode was scanned continuously for 10 cycles before (red) and after (blue) incubation of thrombin with RSD of 0.70% and 0.74%. Figure 3f demonstrates the storage stability of the ECL biosensor by monitoring the ΔECL signal of thrombin over time. Results indicate that the sensor exhibited stable performance, with thrombin signals of 100%, 92.9%, 88.1%, 85.0%, 84.7%, and 83.7% at 1 day, 3 days, 5 days, 7 days, 9 days, and 11 days, respectively.

Meanwhile, the analytical performance of this thrombin biosensor was compared with some previously reported methods (Table S1), such as fluorescence, electrochemistry, electrochemiluminescence, photoelectron chemistry, and chemiluminescence. The prepared ECL biosensor has obvious advantages in terms of detection sensitivity and linear range. In addition, the LOD of the thrombin activity fluorometric assay kit (ELISA) produced by Biovision is only 10 ng/mL, but the LOD of this ECL sensor is 83 pU/mL, providing a significant increase in sensitivity.

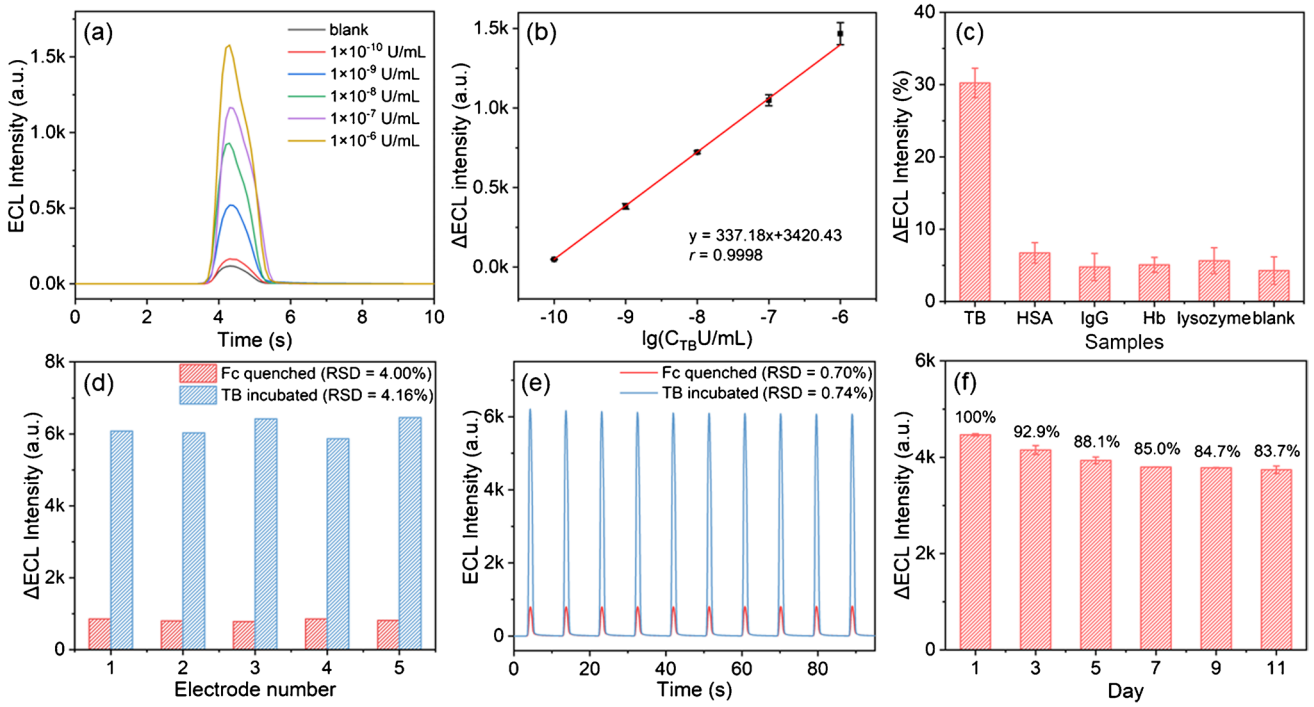

Fig. 3 ECL biosensor methodology investigation diagram. **a** ECL diagrams of different thrombin activities; **b** linear relationship between sensor ΔECL and thrombin activity; **c** Selectivity of the ECL biosensor for thrombin detection by comparing it with different interfering proteins. The concentration of all interfering proteins was 1 mg/mL, and thrombin concentration was 1 μU/mL. **d**, **e** Repeatability of ECL biosensor for 5 electrodes and stability of ECL biosensor scanning for 10 cycles. Fc quenched refers to the state before thrombin addition, TB incubated refers to the state after thrombin addition, thrombin concentration was 1 μU/mL; **f** 11-day storage stability of ECL biosensors; thrombin concentration was 1 μU/mL

Detection of human serum thrombin

To assess the accuracy of the ECL sensor, both the standard addition method and a comparison with a commercial fluorescence kit were employed. As shown in Table 1, the recoveries of ECL method are 104.19%, 103.96%, and 96.25%, with RSD of 3.08%, 1.72%, and 1.81%, respectively. The recoveries of FL method were 98.48%, 101.16%, and 100.44%, with RSD of 1.07%, 0.21%, and 0.13%, respectively. Results from both methods fell within the expected error range. In conclusion, the ECL biosensor can be used to detect thrombin activity in human serum, which has great potential for practical applications.

Screening of potential thrombin inhibitors

Agatroban (Arg) is a direct thrombin inhibitor with an affinity and reversible binding to the thrombin catalytic site [35]. Therefore, Arg was selected as the positive control in the follow-up trial. Figure 4a displays the inhibition curve for Arg, with its IC_{50} value of 0.14 nM calculated using formula (1). This result closely aligns with the previously reported value of 9.36 nM in the literature [36].

$$\text{Inhibitory rate} = \left(1 - \frac{I_x}{I_0}\right) \times 100\% \quad (1)$$

where I_x and I_0 are the ECL intensity with and without inhibitor.

The inhibitory rates of the chosen 10 compounds (Jac, Cin, Iso, Nep, Eup, β-Sit, Ter, α-Ter, L-Cam, and L-Bor) were determined by the constructed ECL biosensor. Fluorescence method was also taken as a comparison. Forty microliters of Arg (10 nM) and 10 compounds (1 μM) were mixed with 10 μL thrombin and incubated at 37 ℃ for 10 min. The mixture was taken to carry the ECL and FL experiments. As shown in Fig. 4b, the inhibition

Table 1 Comparison of recovery rates of thrombin activity in human serum

ECL				FL			
Add (U/mL)	Founded (U/mL)	Recovery (%)	RSD (%, $n=3$)	Add (U/mL)	Founded (U/mL)	Recovery (%)	RSD (%, $n=3$)
1.00×10^{-9}	1.04×10^{-9}	104.19	3.08	1.00×10^{-9}	9.85×10^{-10}	98.48	1.07
1.00×10^{-8}	1.04×10^{-8}	103.96	1.72	1.00×10^{-8}	1.01×10^{-8}	101.16	0.21
1.00×10^{-7}	9.63×10^{-8}	96.25	1.81	1.00×10^{-7}	1.00×10^{-7}	100.44	0.13

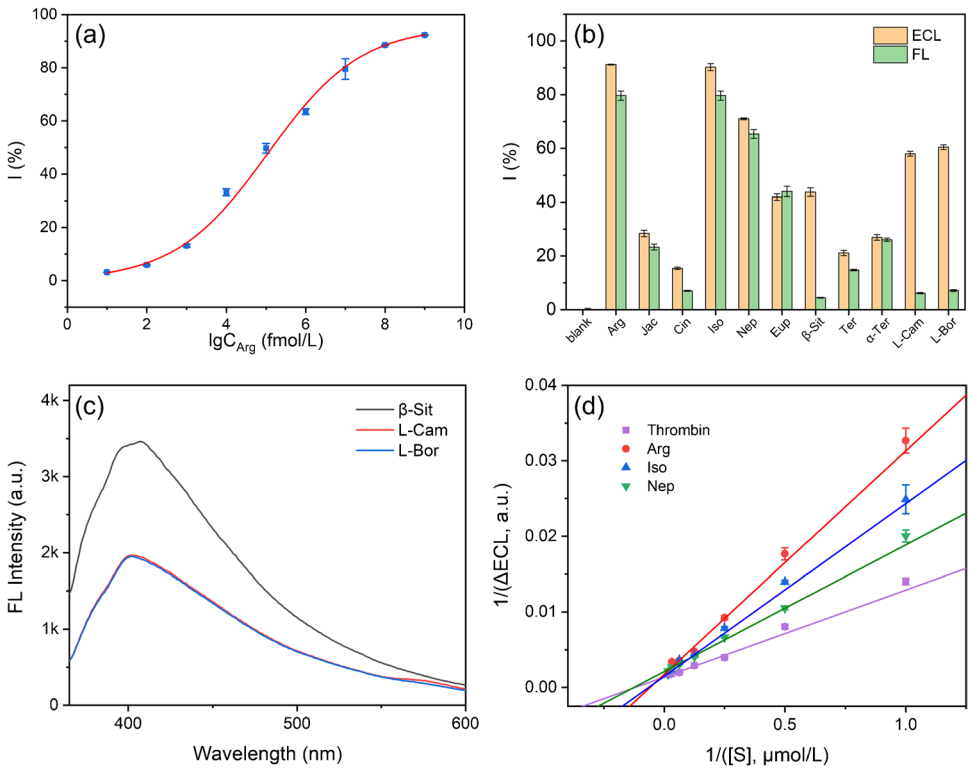

Fig. 4 Screening of thrombin inhibitors. **a** Inhibition curve of positive drug argatroban(Arg) (raw data with bars in blue and fitted curve in red); **b** comparison of thrombin inhibition rates of 11 compounds with ECL and fluorescence (FL) methods; **c** fluorescence emission spectrogram of β-sitosterol (β-Sit), L-camphor (L-Cam), and L-borneol (L-Bor) at excitation wavelength 351 nm; **d** inhibition kinetics of argatroban (Arg), isoquercitrin (Iso) and nepetin (Nep) (fitted curves)

rates of the majority of the compounds measured by both methods are consistent. In ECL results, Iso, Nep, L-Cam, and L-Bor were beyond 50%, especially Iso (90.26%) and Nep (71.01%). However, FL results show that only Iso and Nep were greater than 50%. Remarkably, significant differences were observed in the results of β-Sit, L-Cam, and L-Bor between the ECL and fluorescence methods.

The fluorescence method exhibited considerably lower inhibition rates than the ECL method, potentially due to the influence of fluorescence effects. This hypothesis is supported by the fluorescence emission spectra of β-Sit, L-Cam, and L-Bor at 351 nm excitation, as depicted in Fig. 4c. These three compounds exhibited fluorescence absorption at 351 nm, which could result in false positive fluorescence results and lower inhibition rates.

Type of inhibition

Michaelis–Menten kinetics (K_m) is a commonly used model to describe the enzymatic activity, expressed as the substrate concentration (S) at half of the maximum reaction rate (V_{max}) of the enzyme-catalyzed reaction [37, 38]. However, in the determination of enzyme activity by ECL method, the number of electrons transported, the oxidation peak current (CV), and the ECL intensity are proportional to the substrate concentration. Therefore, K_m should be constructed by the relationship between ECL intensity and substrate concentration [39]. The equation is as follows:

$$I_{(ECL)} = \frac{I_{max(ECL)}[S]}{K_M^{app} + [S]} \quad (2)$$

where $I_{max(ECL)}$ is the maximum obtainable ECL intensity, $[S]$ is the substrate concentration(mol·L^{-1}), and K_M^{app} is the apparent Michaelis – Menten constant.

The results are shown in the Fig. 4d. The K_M^{app} of thrombin is 8.33 μM (purple curve), which is close to the result of 6.14 μM from the literature [40]. This finding suggests the possibility of using the estimated the K_M^{app} value to evaluate thrombin activity. The data indicates that Arg, Iso, and Nep exhibit the same 1/ΔECL value when the substrate concentration is zero, suggesting that these three compounds belong to the class of competitive inhibitors. The inhibition constant K_i was calculated according to the following formula (3).

$$I_{(ECL)} = \frac{I_{max(ECL)}[S]}{K_M^{app}\left(1 + [C]/K_i^{app}\right) + [S]} \quad (3)$$

where $I_{max(ECL)}$ is the maximum obtainable ECL intensity, $[S]$ is the substrate concentration (mol·L^{-1}), K_M^{app} is the apparent Michaelis – Menten constant, $[C]$ is the inhibitor concentration, and K_i^{app} is the inhibition constant.

The K_i^{app} values of Arg, Iso, and Nep are 6.36 nM, 0.91 μM, and 2.18 μM, respectively. The K_i^{app} value of Arg is close to 6.5 nM reported in the literature [41], which proves that the experimental results are reliable.

Molecular docking study

The molecular docking results of Arg, Iso, Nep, L-Cam, L-Bor, and thrombin are shown in Fig. S5. His 57, Trp 60D, Asn 98, Leu 99, Asp102, Ile 174, Asp 189, Ser 195, Gly 216, and Gly 219 are active amino acid residues in the active pocket of thrombin [42]. Arg had the ability to form hydrogen bonds with His 57, Ser 195, and Gly 216 of thrombin. Iso could form hydrogen bonds with the residues of Gly 216 and Gly 219, while Nep could form hydrogen bonds with Asp 189 and Ser 195. Similarly, L-Cam could form hydrogen bonds with Ser 195 and Gly 219, and L-Bor could form hydrogen bonds with Gly 216. These findings demonstrated that Iso, Nep, L-Cam, and L-Bor had the potential to interact with the key amino acid residues located in the thrombin active pocket, indicating their potential as antithrombotic agents.

Conclusion

It has been proved that the ECL sensor based on Ru@MXene and Fc@SiO_2 can be used for determination of α-thrombin activity in human serum and screening direct thrombin inhibitor from compounds. However, the ECL biosensor has limitations in terms of high throughput continuous detection. Future research should focus on improving its capabilities for whole blood detection and spot rapid diagnosis. Additionally, further investigations are necessary to advance the development of these identified inhibitors into viable drug candidates, considering formulation, pharmacokinetics, and toxicology aspects.

Supplementary Information The online version contains supplementary material available at https://doi.org/10.1007/s00604-023-05906-9.

Acknowledgements Financial support from the National Natural Science Foundation of China (81973277, 82273891, 82003709, 22274126) and the National Natural Science Foundation of Shaanxi Province (2021JM-039, 2023-YBSF-262) are gratefully acknowledged.

Data availability The data that support the findings of this study are available from the corresponding author upon reasonable request.

Declarations

Conflict of interest The authors declare no competing interests.

References

1. Davie EW, Kulman JD (2006) An overview of the structure and function of thrombin. Semin Thromb Hemost 32(Suppl 1):3–15. https://doi.org/10.1055/s-2006-939550
2. Shlobin NA, Har-Even M, Itsekson-Hayosh Z, Harnof S, Pick CG (2021) Role of thrombin in central nervous system injury and disease. Biomolecules 11:562–581. https://doi.org/10.3390/biom11040562
3. Sharma T, Brunet JG, Tasneem S, Smith SA, Morrissey JH, Hayward CPM (2021) Thrombin generation abnormalities in commonly encountered platelet function disorders. Int J Lab Hematol 43:1557–1565. https://doi.org/10.1111/ijlh.13638
4. Megia-Fernandez A, Mills B, Michels C, Chankeshwara SV, Dhaliwal K, Bradley M (2017) Highly selective and rapidly activatable fluorogenic thrombin sensors and application in human lung tissue. Org Biomol Chem 15:4344–4350. https://doi.org/10.1039/c7ob00663b
5. Koren O, Azaizah M, Rozner E, Elias M, Turgeman Y (2020) Role of thrombin generation assays in the diagnosis of acute myocarditis and non-ST myocardial infarction. J Thromb Thrombolysis 50:144–150. https://doi.org/10.1007/s11239-019-01996-6
6. Eivazzadeh-Keihan R, Saadatidizaji Z, Maleki A, de la Guardia M, Mahdavi M, Barzegar S, Ahadian S (2022) Recent progresses in development of biosensors for thrombin detection. Biosensors (Basel) 12:767–799. https://doi.org/10.3390/bios12090767
7. Saa L, Diez-Buitrago B, Briz N, Pavlov V (2019) CdS quantum dots generated in-situ for fluorometric determination of thrombin activity. Microchim Acta 186:657–664. https://doi.org/10.1007/s00604-019-3765-2
8. Pochet L, Servais AC, Farcas E, Bettonville V, Bouckaert C, Fillet M (2013) Determination of inhibitory potency of argatroban toward thrombin by electrophoretically mediated microanalysis. Talanta 116:719–725. https://doi.org/10.1016/j.talanta.2013.07.030
9. Osterud B, Latysheva N, Schoergenhofer C, Jilma B, Hansen JB, Snir O (2022) A rapid, sensitive, and specific assay to measure TF activity based on chromogenic determination of thrombin generation. J Thromb Haemost 20:866–876. https://doi.org/10.1111/jth.15606
10. Binder NB, Depasse F, Mueller J, Wissel T, Schwers S, Germer M, Hermes B, Turecek PL (2021) Clinical use of thrombin generation assays. J Thromb Haemost 19:2918–2929. https://doi.org/10.1111/jth.15538
11. Depasse F, Binder NB, Mueller J, Wissel T, Schwers S, Germer M, Hermes B, Turecek PL (2021) Thrombin generation assays are versatile tools in blood coagulation analysis: a review of technical features, and applications from research to laboratory routine. J Thromb Haemost 19:2907–2917. https://doi.org/10.1111/jth.15529
12. Abdussalam A, Xu G (2022) Recent advances in electrochemiluminescence luminophores. Anal Bioanal Chem 414:131–146. https://doi.org/10.1007/s00216-021-03329-0
13. Yang J, Xia Q, Guo L, Luo F, Dong Y, Qiu B, Lin Z (2020) A highly sensitive signal-on biosensor for microRNA 142–3p based on the quenching of $Ru(bpy)_3^{2+}$-TPA electrochemiluminescence by carbon dots and duplex specific nuclease-assisted target recycling amplification. Chem Commun (Camb) 56:6692–6695. https://doi.org/10.1039/c9cc09706f
14. Gao X, Gu X, Min Q, Wei Y, Tian C, Zhuang X, Luan F (2022) Encapsulating $Ru(bpy)_3^{2+}$ in an infinite coordination polymer network: towards a solid-state electrochemiluminescence sensing platform for histamine to evaluate fish product quality. Food Chem 368:130852. https://doi.org/10.1016/j.foodchem.2021.130852
15. Devaraj M, Rajendran S, Hoang TKA, Soto-Moscoso M (2022) A review on MXene and its nanocomposites for the detection of toxic inorganic gases. Chemosphere 302:134933. https://doi.org/10.1016/j.chemosphere.2022.134933
16. Hou MZ, Chen LL, Chang C, Zan JF, Du SM (2021) Pharmacokinetic and tissue distribution study of eight volatile constituents in rats orally administrated with the essential oil of Artemisiae Argyi Folium by GC-MS/MS. J Chromatogr B 1181:122904. https://doi.org/10.1016/j.jchromb.2021.122904
17. Ma Q, Tan D, Gong X, Ji H, Wang K, Lei Q, Zhao G (2022) An extract of Artemisia Argyi leaves rich in organic acids and flavonoids promotes growth in BALB/c mice by regulating intestinal flora. Animals (Basel) 12:1519–1536. https://doi.org/10.3390/ani12121519
18. Huang W, Wang Y, Liang WB, Hu GB, Yao LY, Yang Y, Zhou K, Yuan R, Xiao DR (2021) Two birds with one stone: surface functionalization and delamination of multilayered $Ti_3C_2T_x$ MXene by grafting a ruthenium(II) complex to achieve conductivity-enhanced electrochemiluminescence. Anal Chem 93:1834–1841. https://doi.org/10.1021/acs.analchem.0c04782
19. Dong YP, Chen G, Zhou Y, Zhu JJ (2016) Electrochemiluminescent sensing for caspase-3 activity based on $Ru(bpy)_3^{2+}$-doped silica nanoprobe. Anal Chem 88:1922–1929. https://doi.org/10.1021/acs.analchem.5b04379
20. Alhabeb M, Maleski K, Anasori B, Lelyukh P, Clark L, Sin S, Gogotsi Y (2017) Guidelines for synthesis and processing of two-dimensional titanium carbide ($Ti_3C_2T_X$ MXene). Chem Mater 29:7633–7644. https://doi.org/10.1021/acs.chemmater.7B02847
21. Huang H, Xie S, Deng L, Yuan J, Yue R, Xu J (2022) Fabrication of rGO/MXene-Pd/rGO hierarchical framework as high-performance electrochemical sensing platform for luteolin detection. Microchim Acta 189:59–69. https://doi.org/10.1007/s00604-021-05132-1
22. Zhang J, Kerr E, Usman KAS, Doeven EH, Francis PS, Henderson LC, Razal JM (2020) Cathodic electrogenerated chemiluminescence of tris(2,2'-bipyridine)ruthenium(ii) and peroxydisulfate at pure $Ti_3C_2T_X$ MXene electrodes. Chem Commun (Camb) 56:10022–10025. https://doi.org/10.1039/d0cc02993a
23. Karaman C, Karaman O, Atar N, Yola ML (2021) Electrochemical immunosensor development based on core-shell high-crystalline graphitic carbon nitride@carbon dots and $Cd_{0.5}Zn_{0.5}S$/d-$Ti_3C_2T_x$ MXene composite for heart-type fatty acid–binding protein detection. Microchim Acta 188:182–197. https://doi.org/10.1007/s00604-021-04838-6
24. Sun Y, Zhang Y, Zhang H, Liu M, Liu Y (2020) Integrating highly efficient recognition and signal transition of g-C_3N_4 embellished Ti_3C_2 MXene hybrid nanosheets for electrogenerated chemiluminescence analysis of protein kinase activity. Anal Chem 92:10668–10676. https://doi.org/10.1021/acs.analchem.0c01776
25. Koyappayil A, Chavan SG, Mohammadniaei M, Go A, Hwang SY, Lee M-H (2020) β-Hydroxybutyrate dehydrogenase decorated MXene nanosheets for the amperometric determination of β-hydroxybutyrate. Microchim Acta 187:277–284. https://doi.org/10.1007/s00604-020-04258-y
26. Han M, Yin X, Wu H, Hou Z, Song C, Li X, Zhang L, Cheng L (2016) Ti_3C_2 MXenes with modified surface for high-performance electromagnetic absorption and shielding in the X-band. ACS Appl Mater Interfaces 8:21011–21019. https://doi.org/10.1021/acsami.6b06455
27. Yang J, Deng C, Zhong W, Peng G, Zou J, Lu Y, Gao Y, Li M, Zhang S, Lu L (2023) Electrochemical activation of oxygen vacancy-rich TiO_2@MXene as high-performance electrochemical sensing platform for detecting imidacloprid in fruits and vegetables. Microchim Acta 190:146–157. https://doi.org/10.1007/s00604-023-05734-x

28. Halim J, Cook KM, Naguib M, Eklund P, Barsoum MW (2016) X-ray photoelectron spectroscopy of select multi-layered transition metal carbides (MXenes). Appl Sur Sci 362:406–417. https://doi.org/10.1016/j.apsusc.2015.11.089
29. Tang X, Zhou Z, Jiang Y, Wang Q, Sun Q, Zu L, Gao X, Lian H, Cao M, Cui X (2022) MXene enhanced the electromechanical performance of a nafion-based actuator. Materials (Basel) 15:2833–2844. https://doi.org/10.3390/ma15082833
30. Du J-F, Chen J-S, Liu X-P, Mao C-J, Jin B-K (2022) Coupled electrochemiluminescent and resonance energy transfer determination of microRNA-141 using functionalized Mxene composite. Microchim Acta 189:264–273. https://doi.org/10.1007/s00604-022-05359-6
31. Wang D, Li Y, Lin Z, Qiu B, Guo L (2015) Surface-enhanced electrochemiluminescence of Ru@SiO_2 for ultrasensitive detection of carcinoembryonic antigen. Anal Chem 87:5966–5972. https://doi.org/10.1021/acs.analchem.5b01038
32. Zhai H, Wang Y, Yin J, Zhang Y, Guo Q, Sun X, Guo Y, Yang Q, Li F, Zhang Y (2022) Electrochemiluminescence biosensor for determination of lead(II) ions using signal amplification by Au@SiO_2 and tripropylamine-endonuclease assisted cycling process. Microchim Acta 189:317–328. https://doi.org/10.1007/s00604-022-05429-9
33. Ding L, Zou H, Lu J, Liu H, Wang S, Yan H, Li Y (2022) Enhancing proton conductivity of nafion membrane by incorporating porous Tb-metal-organic framework modified with nitro groups. Inorg Chem 61:16185–16196. https://doi.org/10.1021/acs.inorgchem.2c02782
34. Hu S, Zhu H, Liu S, Xiang J, Sun W, Zhang L (2012) Electrochemical detection of rutin with a carbon ionic liquid electrode modified by nafion, graphene oxide and ionic liquid composite. Microchim Acta 178:211–219. https://doi.org/10.1007/s00604-012-0811-8
35. Escolar G, Bozzo J, Maragall S (2006) Argatroban: a direct thrombin inhibitor with reliable and predictable anticoagulant actions. Drugs Today (Barc) 42:223–236. https://doi.org/10.1358/dot.2006.42.4.953588
36. Li M, Ren Y (2015) Synthesis and biological evaluation of some new 2,5-substituted 1-Ethyl-1H-benzoimidazole fluorinated derivatives as direct thrombin inhibitors. Arch Pharm (Weinheim) 348:353–365. https://doi.org/10.1002/ardp.201400463
37. Seibert E, Tracy TS (2021) Fundamentals of enzyme kinetics: michaelis-menten and non-michaelis-type (atypical) enzyme kinetics. Methods Mol Biol 2342:3–27. https://doi.org/10.1007/978-1-0716-1554-6_1
38. Fan R, Tian J, Wang H, Wang X, Zhou P (2022) Sensitive colorimetric assay of hydrogen peroxide and glucose in humoral samples based on the enhanced peroxidase-mimetic activity of NH_2-MIL-88-derived FeS_2@CN nanocomposites compared to its precursors. Microchim Acta 189:427–437. https://doi.org/10.1007/s00604-022-05525-w
39. Ferraraccio LS, Di Lisa D, Pastorino L, Bertoncello P (2022) Enzymes encapsulated within alginate hydrogels: bioelectrocatalysis and electrochemiluminescence applications. Anal Chem 94:16122–16131. https://doi.org/10.1021/acs.analchem.2c03389
40. Xu Z, Liu R, Guan H (2017) Dual-target inhibitor screening against thrombin and factor Xa simultaneously by mass spectrometry. Anal Chim Acta 990:1–10. https://doi.org/10.1016/j.aca.2017.07.063
41. Zavyalova E, Kopylov A (2015) Multiple inhibitory kinetics reveal an allosteric interplay among thrombin functional sites. Thromb Res 135:212–216. https://doi.org/10.1016/j.thromres.2014.11.005
42. Shi Y, Sun W, Pan X, Hou X, Wang S, Zhang J (2020) Establishment of thrombin affinity column (TAC)-HPLC-MS/MS method for screening direct thrombin inhibitors from radix salviae miltiorrhiae. J Chromatogr B 1139:121894. https://doi.org/10.1016/j.jchromb.2019.121894